J. Archaeol. Sci. **21**, 839 (1994).
37. Associated sediment collected less than 10 cm from the in situ teeth was collected for estimation of beta and gamma dose rates. We used the in-situ sediment collected near 95297 at Ngandong to estimate dose rates to museum teeth 94762 and 95393 from Ngandong, and 94761 from Sambungmacan. The internal dose rates for all teeth are high, and slight variations in the composition of enclosing sediment used for museum samples would have negligible effect on the calculated ages. The ESR ages (Table 1) were calculated using the standard program DATA of R. Grün. The ESR ages were also calculated using new ESR dating software called ROSY (B. J. Brennan, W. J. Rink, E. L. McGuirl, H. P. Schwarcz, W. V. Prestwich, *Radia. Meas.*, in press) using "One-Group" theory for beta dose attenuation in enamel. Using this method, both the EU- and LU-ESR ages are approximately 4000 years older than those using the DATA program. The mean EU age for Ngandong would be 31.4 ± 3.5 ka and agrees more closely with the U-series ages of 30 to 40 ka for the stripped enamels U-series ages.
38. C. R. McKinney, thesis, Southern Methodist University (1991).
39. R. Grün and F. McDermott, *Quat. Sci. Rev. (Quat. Geochronol.)* **13**, 121 (1994).
40. R. Grün and L. Taylor, *Ancient Thermolumia* **14**, 21 (1996).
41. R. Grün, H. P. Schwarcz, J. Chadam, *Nucl. Tracks* **14**, 237 (1988).
42. F. McDermott, R. Grün, C. B. Stringer, C. J. Hawkesworth, *Nature* **363**, 252 (1993).
43. E. Tamarat, N. Thouveny, M. Taieb, N. D. Opdyke, *Palaeogeogr. Palaeoclimatol. Palaeoecol.* **114**, 273 (1994).
44. C. Tiemei and Y. Sixun, *Archaeometry* **30**, 59 (1988).
45. Y. Sixun, C. Tiemei, G. Shijun, *Acta Anthropol. Sin.* **5**, 179 (1986); more recently, P. Brown [*Philos. Trans. R. Soc.* (1993)] has argued that there is no clear association of this date with the hominid skull at Liujiang.
46. Y. Sixun, C. Tiemei, G. Shijun, H. Yanqui, *Acta Anthropol. Sin.* **10**, 189 (1991).
47. S. Guanjun and J. Linhong, *ibid.*, p. 273; R. Ku, personal communication
48. S. C. Antón, in preparation; P. Brown, *Archaeol. Oceania* **16**, 156 (1981); *Terra Aust.* **13** (1989); N. W. G. Macintosh and S. L. Larnach, in *The Origin of the Australians*, R. L. Kirk and A. G. Thorne, Eds. (Humanities, Atlantic Highlands, NJ, 1976), p. 113; S. Webb, *Paleopathology of Aboriginal Australians: Health and Disease of a Hunter-Gatherer Continent* (Cambridge Univ. Press, Cambridge, 1995); N. W. G. Macintosh and S. L. Larnach, *Arch. Phys. Anthropol. Oceania* **7**, 1 (1972). and refs. 1 and 7 therein.
49. M. M. Lahr, *J. Hum. Evol.* **26**, 23 (1994).
50. F. C. Howell, in *Origins of Anatomically Modern Humans*, M. H. Nitecki and D. V. Nitecki, Eds. (Plenum, New York, 1994), p. 253.
51. J. H. Relethford and C. B. Stringer, in preparation.
52. H. P. Schwarcz and R. Grün, *Philos. Trans. R. Soc. London B* **337**, 145 (1992); H. Valladas *et al.*, *Nature* **331**, 614 (1988).
53. P. Storm, *Scri. Geol.* **110**, 1 (1996); R. Shutler, in *Felicitation for R. P. Soejdono*, in press.
54. J. M. Bowler, A. G. Thorne, H. A. Polach, *Nature* **240**, 48 (1972).
55. D. R. Brothweil, *J. Sarawak Mus.* **323**, 1 (1960). There appears to be some question as to whether the ^{14}C dates are physically related to the Niah Cave hominid remains.
56. L. Groube, J. Chappell, J. Muke, D. Price, *Nature* **324**, 453 (1986).
57. R. G. Roberts, R. Jones, M. A. Smith, *ibid.* **345**, 153 (1990); P. G. Bahn, *ibid.* **383**, 577 (1996); R. L. K. Fullager, D. M. Prince, L. M. Head, *Antiquity*, in press.
58. I. Tattersall and J. Schwartz, *Proc. Nat. Acad. Sci. U.S.A.*, in press.
59. Predecessors to Neandertals first appear by the Mid-Pleistocene in Western Europe [E. Carbonell *et al.*, *Science* **269**, 826 (1995); H. de Lumley and M.-A. de Lumley, *C. R. Acad. Sci. Paris* **272**, 1729 (1971)], whereas classical Neandertals persist until nearly 30 ka [J. K. Kozlowski, *Excavations in the Bacho Kiro Cave, Bulgaria (final report)* (Paristwowe Wydaruyn-ictwo, Naukowe, Warsaw, 1982); J. L. Bischoff, N. Soler, J. Maroto, R. J. Julia, *J. Archaeol. Sci.* **16**, 553 (1989)], overlapping in time and space with anatomically modern humans that first appear in Europe and Western Asia around 40 to 50 ka [J. J. Hublin, C. Barroso Ruiz, P. Medina Lara, M. Fontugni, J.-L. Reyss, *C. R. Acad. Sci. Paris* **321**, 931 (1995); J. J. Hublin, F. Spoor, M. Braun, F. Zonneveld, S. Condemi, *Nature* **381**, 224 (1996); C. B. Stringer and R. Grün, *ibid.* **351**, 701 (1991); M. H. Wolpoff and D. Frayer, *ibid.* **356**, 200 (1992); D. Frayer, in *Continuity or Replacement: Controversies in* Homo sapiens Evolution, G. Bräuer and F. H. Smith, Eds. (Balkema, Rotterdam, 1992), pp. 179–188].
60. This project was supported by NSF (SBR-9405320) and L. S. B. Leakey Foundation grants to C.C.S. and G.H.C. Partial support for ESR and U-series dating was by NSF grant SBR-9410906 to H. Schwarcz; laboratory assistance was by K. Googer and J. Johnson. We would like to thank T. Jacob and F. Aziz for their help with field arrangements and museum specimens and C. B. Stringer, who provided valuable comments on an earlier draft of this manuscript.

26 June 1996; accepted 23 October 1996

Dynamical Signature of the Mott-Hubbard Transition in Ni(S,Se)$_2$

A. Husmann, D. S. Jin,* Y. V. Zastavker,† T. F. Rosenbaum,‡ X. Yao, J. M. Honig

The transition metal chalcogenide Ni(S,Se)$_2$ is one of the few highly correlated, Mott-Hubbard systems without a strong first-order structural distortion that normally cuts off the critical behavior at the metal-insulator transition. The zero-temperature (T) transition was tuned with pressure, and significant deviations were found near the quantum critical point from the usual $T^{1/2}$ behavior of the conductivity characteristic of electron-electron interactions in the presence of disorder. The transport data for pressure and temperature below 1 kelvin could be collapsed onto a universal scaling curve.

Disorder can turn a good metal into an insulator. Alternatively, strong interactions between electrons can split the half-filled band of a crystalline metal and open an insulating gap. In the first limit, a critical degree of disorder localizes the electrons through quantum interference and leads to the continuous Anderson transition at $T = 0$. In the correlation-driven scenario, a metal-insulator (MI) transition occurs when the ratio of the intrasite Coulomb repulsion to the bandwidth is of order unity. This Mott-Hubbard picture applies at nonzero temperature and is usually first order, often with coincident electronic, magnetic, and structural transitions.

This dichotomy between the Anderson and the Mott-Hubbard limits suffuses theoretical treatments of the MI transition (*1*). However, blending correlations and disorder can be more amenable to theoretical exposition, with the possibility of a well-defined order parameter (*2*). Experimental characterization of the critical behavior requires high-resolution measurements in the $T \rightarrow 0$ limit on materials that must satisfy a severe set of constraints: (i) true statistical disorder without the chemical segregation that gives rise to classical percolation effects; (ii) strong electron-electron interactions, but only a modest band gap to permit tuning; and (iii) strong electron-electron interactions, but no first-order structural instability at the MI transition.

It is this last constraint that may be the most restrictive in the highly correlated limit. For example, it is possible to deconvolute the effects of correlations and disorder at the $T = 0$ MI transition in the Mott-Hubbard system vanadium sesquioxide (*3*), but there are no actual divergences. The critical behavior at the transition is cut off by a sudden, symmetry-breaking, monoclinic distortion. In contrast, the transition-metal chalcogenide $NiS_{2-x}Se_x$ is one of the select few Mott-Hubbard materials (*4*) without a structural instability tied to the localization of charge (*5*). The $T = 0$ MI transition can be tuned with pressure, which offers an experimental approach to the mixture of statics and dynamics at a quantum critical point.

Nickel diselenide, $NiSe_2$, is a good metal while nickel disulfide, NiS_2, is a Mott insulator, whose half-filled narrow $3d$ e_g band is split by the Hubbard U, the intrasite Coulomb repulsion, with a band gap < 1 eV (*6*). Substitution of Se for S drives the system metallic, with a MI transition seen as a function of temperature for $NiS_{2-x}Se_x$ in the narrow range $0.47 < x <$

A. Husmann, D. S. Jin, Y. V. Zastavker, T. F. Rosenbaum, The James Franck Institute and Department of Physics, The University of Chicago, Chicago, IL 60637, USA.
X. Yao and J. M. Honig, Department of Chemistry, Purdue University, West Lafayette, IN 47907, USA.

*Present address: Joint Institute for Laboratory Astrophysics, University of Colorado, Boulder, CO 80309, USA.
†Present address: Department of Physics, Massachusetts Institute of Technology, Cambridge, MA 02139, USA.
‡To whom correspondence should be addressed.

0.54 (*7*, *8*). Both the metal and the insulator have a pyrite structure, with some reports of a volume change of the unit cell at the MI transition (*9*). The addition of Se increases the bandwidth W through covalent mixing without moving the system away from half-filling. In addition to decreasing the effective interaction strength U/W, Se substitution simultaneously introduces random disorder on the anion sites. Applied hydrostatic pressure also can increase W, with the empirical relation that 1% Se chemical pressure corresponds to 1.2-kbar external pressure (*10*)

Single crystals of $NiS_{2-x}Se_x$ were grown by the Te flux method, as opposed to the more usual chemical vapor transport operation involving Cl_2 or Br_2 as the transport agent (*8*, *11*). Unlike chlorine or bromine, the heavier tellurium resists incorporation into the crystal. This procedure removes potential complications from excess impurity concentrations (*12*), a serious constraint for electrical measurements in the insulator, but undesirable as well in the metal. The amount of Se substitution x is determined from x-ray diffraction measurements of the lattice parameter by using Vegard's law which is accurately obeyed (*13*). Ion microprobe studies indicate an actual stoichiometry $Ni(S,Se)_{2-\delta}$, with $\delta = 0.03 \pm 0.01$ across the breadth of a crystal. We performed four-probe resistivity measurements using an ac bridge technique in the ohmic and frequency-independent limits. While the error on the relative values of the resistivity ρ are less than 0.01%, there is an absolute uncertainty of 25% because of the small size of the crystals (from 0.3 to 0.7 mm on a side) and the macroscopic silver paint contacts. We applied hydrostatic pressure P with a BeCu pressure cell designed to fit into the top-loading confines of an Oxford Model 200 dilution refrigerator. A chip of $(V_{0.99}Ti_{0.01})_2O_3$ inside the cell serves as a sensitive manometer through its own MI transition (*14*).

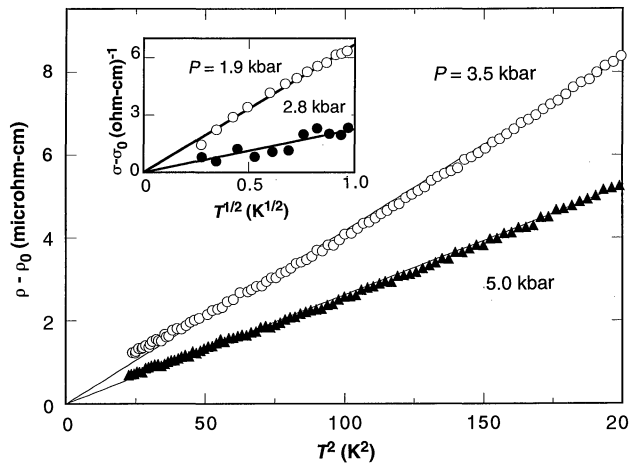

Fig. 2. The large T^2 dependence of the resistivity ρ with slope increasing at the approach to the MI transition indicates a greatly enhanced electronic effective mass. Inset: The effective mass enhancement is revealed as well by the changing slope of the $T^{1/2}$ dependence of the conductivity σ for $T < 1$ K, characteristic of electron-electron interactions in the presence of disorder.

We started with $NiS_{1.56}Se_{0.44}$ crystals just on the insulating side of the MI boundary and drove the system metallic with pressure. We plot in Fig. 1 the effective $T \rightarrow 0$ conductivity, $\sigma(T = 0.05\ K)$, versus P for two such samples, where ~ 1 $(\text{milliohm-cm})^{-1}$ is the characteristic Mott conductivity. We fit the data to the standard scaling form for a continuous transition, $\sigma(0) \sim t^{\mu}$, where $t \equiv (P - P_c)/P_c$ is the normalized distance from the quantum critical point, and we find $\mu = 1.1 \pm 0.2$ with $P_c = 1.51$ (filled circles) and 1.67 kbar (open circles), respectively. These values of P_c correspond to the expected $x_c = 0.47$; the difference of 0.16 kbar corresponds to a difference in $x \sim 0.003$. If the chemical pressure from the Se substitution is included in P_c, our values for the dimensionless distance t would be more than an order of magnitude smaller.

The metallic phase is highly correlated, as demonstrated by a large T^2 term in the resistivity (Fig. 2). The increasing slope with decreasing P reflects a strong enhancement in the effective mass as the MI transition is approached from above, consonant with the traditional Brinkman-Rice picture of an effective mass divergence driving the transition (*15*). At $P = 3.5$ kbar, the slope of 0.042 (microhm-cm/K^2) is equivalent to that of barely metallic V_2O_3 (*3*, *16*).

At very low temperatures ($T < 1$ K), we observe a $T^{1/2}$ form of the conductivity characteristic of electron-electron interactions in the presence of disorder (*1*, *17*) whose increasing slope with decreasing P is a parallel indicator of a pronounced effective mass enhancement (Fig. 2, inset). As in the case of many highly correlated metals on the verge of a MI transition, the ground state is antiferromagnetic. $NiS_{2-x}Se_x$ has the unusual distinction, however, and for our purposes the added advantage, of a P-T phase diagram where for decreasing T at fixed P the sequence paramagnetic insulator to antiferromagnetic insulator to antiferromagnetic metal can occur. Well below the

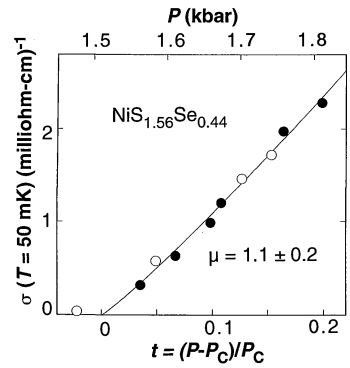

Fig. 1. The $T \rightarrow 0$ conductivity σ_0 as a function of reduced pressure t for two crystals with $P_c = 1.51$ kbar (filled circles) and $P_c = 1.67$ kbar (open circles) at the MI transition. The conductivity falls smoothly to zero, $\sigma_0 \sim t^{\mu}$, where 1 $(\text{milliohm-cm})^{-1}$ is of order the Mott conductivity.

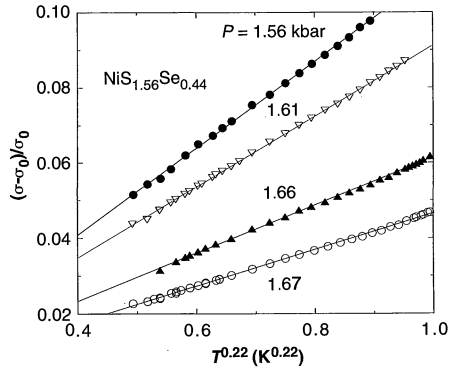

Fig. 3. Near the quantum critical point ($P_c = 1.51$ kbar), a new functional form describes the temperature-(frequency-)dependent conductivity. This first-order correction to σ_0 at P_c has a $T^{0.22 \pm 0.02}$ dependence, an exponent most accurately determined by dynamical scaling (Fig. 4).

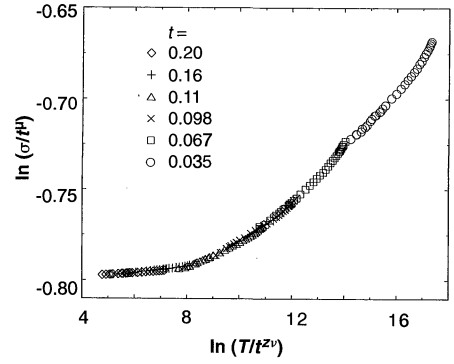

Fig. 4. Dynamical scaling curve for the six closest reduced pressures t to the $T = 0$ Mott-Hubbard MI transition. The ability to collapse the data onto a universal curve reflects the measurable influence of the quantum critical point.

Néel temperature, the spin fluctuations are frozen out and both the T^2 and the $T^{1/2}$ electron-correlation terms in the resistivity can reflect the true behavior of the electronic effective mass.

We focus in Fig. 3 on the low-temperature behavior of the conductivity for pressures very near the $T = 0$ MI transition. At pressures more than 0.2 kbar above the transition, we observed the usual $T^{1/2}$ form. However, for $P \approx P_c$, the influence of the critical point becomes apparent. A new functional form, $(\sigma - \sigma_0) \sim T^{0.22}$, describes best the dynamical (finite T or ω) response. This unusual exponent follows either from a simple two-parameter least squares fit (0.20 ± 0.07) for $0.035\ K < T < 0.800\ K$ or more precisely (0.22 ± 0.02) from the dynamical scaling analysis discussed below.

Wegner (*18*) proposed a dynamical scaling picture of the $T = 0$ MI transition for noninteracting electrons in a random potential. When these ideas are extended to include interactions in the presence of disorder (*2*, *19*), the electrical conductivity is given by:

$$\sigma(t,T) = b^{-x_\sigma} f(tb^{1/\nu}, Tb^{z}) \qquad (1a)$$

where x_σ is an unknown exponent, z is the dynamical scaling exponent, ν is the correlation length exponent, f is a scaling function, and b is an arbitrary scale parameter. It follows that:

$$\sigma(t, T = 0) \sim t^{\mu} \text{ and } \sigma(t \to 0, T) \sim T^{x_\sigma/z}, \qquad (1b)$$

with the conductivity exponent $\mu = \nu x_\sigma$. By Eq. 1a, σ/t^{μ} should be only a function of $T/t^{z\nu}$.

We collapse our conductivity data (*20*) closest to the transition onto such a scaling plot in Fig. 4. The ratio $z\nu/\mu = z/x_\sigma = 4.6 \pm 0.4$ determines the exponent for the first-order correction to σ_0. We then find $\mu = 1.1 \pm 0.2$ by fitting the extracted values of $\mu \ln(t)$ as a function of P, a result in accord with the analysis of the unscaled data of Fig. 1.

Although the data closest to P_c collapse onto a universal scaling curve (Fig. 4), and there is no structural distortion at P_c, we observe a small hysteresis (~1 K) on thermal cycling through the transition (*21*). Presumably, the MI transition is weakly first order, but sufficiently weakly first order to be effectively continuous and to permit the influence of the quantum critical point to emerge. In our efforts to quantify the interplay of statics and dynamics in high-quality single crystals of $NiS_{1.56}Se_{0.44}$, we found that the static critical exponent for the conductivity, $\mu = 1.1 \pm 0.2$, has the value common to most $T \to 0$ continuous MI transitions (*1*), but that the value $x_\sigma/z = 0.22 \pm 0.02$ is unexpected. For noninteracting electrons in three dimensions ($d = 3$), Wegner scaling gives (*18*) $\mu = \nu$ and $x_\sigma/z = 1/3$. Including the effects of electron-electron interactions at the level of a Landau theory for $d > 6$, Kirkpatrick and Belitz (*2*, *22*) find $x_\sigma/z = 2/3$ for $\mu = 1$. By analogy to the random-field Ising model, these authors also point out that hyperscaling should be violated (*22*). An additional experiment would be required to determine if hyperscaling holds for the $Ni(S,Se)_2$ system.

REFERENCES AND NOTES

1. For recent reviews, see P. A. Lee and T. V. Ramakrishnan, *Rev. Mod. Phys.* **57**, 287 (1985), and D. Belitz and T. R. Kirkpatrick, *ibid.* **66**, 261 (1994).
2. T. R. Kirkpatrick and D. Belitz, *Phys. Rev. Lett.* **73**, 862 (1994).
3. S. A. Carter *et al.*, *Phys. Rev. B* **48**, 16841 (1993); T. F. Rosenbaum, in *The Metal-Nonmetal Transition Revisited*, P. P. Edwards and C. N. Rao, Eds. (Taylor and Francis, London, 1995), pp. 105–127.
4. Although $NiS_{2-x}Se_x$ has charge-transfer characteristics, it is commonly analyzed within a Mott-Hubbard framework. See, for example, J. Zaanen, G. A. Sawatzky, J. W. Allen, *Phys. Rev. Lett.* **55**, 418 (1985); A. Y. Matsuura *et al.*, *Phys. Rev. B* **53**, R7584 (1996).
5. H. S. Jarrett *et al.*, *Mater. Res. Bull.* **8**, 877 (1973); F. Gautier *et al.*, *Phys. Lett. A* **53**, 31 (1975); G. Krill and A. Anamou, *J. Phys. Chem. Solids* **41**, 531 (1980); S. Sudo *et al.*, *J. Phys. Soc. Jpn.* **55**, 1806 (1986); X. Yao *et al.*, in *The Metal-Nonmetal Transition Revisited*, P. P. Edwards and C. N. Rao, Eds. (Taylor and Francis, London, 1995), pp. 129–142.
6. For a review, see J. A. Wilson, in *The Metallic and Nonmetallic States of Matter*, P. P. Edwards and C. N. Rao, Eds. (Taylor and Francis, London, 1985), pp. 215–260.
7. R. J. Bouchard, J. L. Gillson, H. S. Jarrett, *Mater. Res. Bull.* **8**, 489 (1973); H. S. Jarrett *et al.*, *ibid.*, p. 877; P. Kwizera, M. S. Dresselhaus, D. Adler, *Phys. Rev. B* **21**, 2328 (1980).
8. X. Yao, T. Hogan, C. Kannewurf, J. M. Honig, preprint.
9. S. Endo, T. Mitsui, T. Miyadai, *Phys. Lett. A* **46**, 29 (1973); T. Miyadai, M. Saitoh, Y. Tazuke, *J. Magn. Magn. Mater.* **104–107**, 1953 (1992).
10. N. Mori *et al.*, *Solid State Physics under Pressure: Recent Advances with Anvil Devices* (Reidel, Dordrecht, 1985), p. 247; J. A. Wilson and G. D. Pitt, *Philos. Mag.* **23**, 1297 (1971).
11. X. Yao and J. M. Honig, *Mater. Res. Bull.* **29**, 709 (1994).
12. K. Kourtakis *et al.*, *J. Solid State Chem.* **76**, 186 (1988).
13. D. D. Klemm, *N. Jahrb. Mineral. Monatsh. J.* **1962**, 32 (1962).
14. T. F. Rosenbaum, S. A. Carter, J. M. Honig, *Rev. Sci. Instrum.* **67**, 617 (1996).
15. W. F. Brinkman and T. M. Rice, *Phys. Rev. Lett.* **27**, 941 (1971); X. Y. Zhang, M. J. Rozenberg, G. Kotliar, *ibid.* **70**, 1666 (1993); Y. Tokura *et al.*, *ibid.*, p. 2126.
16. D. B. McWhan and T. M. Rice, *ibid.* **22**, 887 (1969).
17. B. L. Altshuler, A. G. Aronov, P. A. Lee, *ibid.* **44**, 1288 (1980); T. F. Rosenbaum *et al.*, *ibid.* **46**, 568 (1981).
18. F. J. Wegner, *Z. Phys. B* **25**, 327 (1976).
19. A. M. Finkel'stein, *Sov. Phys. JETP* **57**, 97 (1983); *Sov. Sci. Rev. A* **14**, 1 (1990); C. Castellani, G. Kotliar, P. A. Lee, *Phys. Rev. Lett.* **59**, 323 (1987).
20. The scaling curve is very sensitive to the exact values of t because the temperature dependence of the conductivity is so much smaller than its pressure dependence. Therefore, we allow the product of the normalized pressure and the conductivity exponent, $\mu \ln(t)$, to float, consistent with the uncertainty in our pressure measurement, ±0.03 kbar. By using a log-log scaling plot of σ/t^{μ} versus $T/t^{z\nu}$, we can determine the best ratio of the exponents $z\nu/\mu$ for the optimal collapse of the data, where no pressure is actually adjusted by more than 0.02 kbar. The kink at $\ln(T/t^{z\nu}) \approx 14$ depends on only one data set and is probably not significant.
21. See also S. Sudo, *J. Magn. Magn. Mater.* **114**, 57 (1992).
22. T. R. Kirkpatrick and D. Belitz, *Phys. Rev. Lett.* **74**, 1178 (1995).

23. We are grateful to D. Belitz for sharing his results prior to publication and to E. Shung for helpful discussions. The work at the University of Chicago was supported by NSF grant DMR95-07873. Y.V.Z. acknowledges support from the NSF REU Program. The work at Purdue University was supported by NSF grant DMR92-22986.

22 July 1996; accepted 22 October 1996

Hf-W Isotopic Evidence for Rapid Accretion and Differentiation in the Early Solar System

Der-Chuen Lee and Alex N. Halliday

The time scales over which inner solar system objects accreted and differentiated are unclear because the isotopic systems of many meteorites are disturbed. ^{182}Hf decays to ^{182}W with a half-life of 9 million years and is a particularly useful chronometer because both elements are highly refractory and immobile. Tungsten isotopic data for IIA, IIIA, IVA, and anomalous iron meteorites and H, L, and LL chondrites indicate that their parent bodies accreted rapidly and segregated metal within just a few million years.

Radionuclides with half-lives on the order of 10^6 to 10^8 years can provide information on the earliest history of the solar system and the nature of the nucleosynthetic events that contributed material to the molecular cloud that collapsed to form the solar nebula (*1*–*4*). Among various short-lived chronometers, ^{182}Hf-^{182}W [half life, $t_{1/2}$, of 9 million years (m.y.)] is particularly useful for determining the timing of metal-silicate differentiation (such as core formation) in planets and planetesimals (*5*–*7*). Both Hf and W are highly refractory elements and thus are expected to be in chondritic proportions in much of the solar system, but Hf is strongly lithophile whereas W is moderately siderophile such that the Hf/W ratio in silicate phases will be

Department of Geological Sciences, University of Michigan, Ann Arbor, MI 48109–1063 USA.